

Electrosteric Stabilization of Colloidal Dispersions

Gerhard Fritz,[†] Volker Schädler,[†] Norbert Willenbacher,^{*,†} and
Norman J. Wagner[‡]

Polymer Research Division, BASF Aktiengesellschaft, D-67056 Ludwigshafen, Germany, and
Center for Molecular and Engineering Thermodynamics, Department of Chemical Engineering,
University of Delaware, Newark, Delaware 19716

Received December 13, 2001. In Final Form: April 22, 2002

The electrosteric stabilization of model colloidal dispersions is quantified through high-frequency rheometry and complementary techniques. Model aqueous dispersions with a poly(butyl acrylate)–polystyrene core and a layer of poly(methacrylic acid) grafted onto the surface are prepared and characterized. The influence of pH, electrolyte concentration, and amount of polymer in the stabilizing layer on dispersion stability and rheology is investigated. Dynamic light scattering, electrophoretic mobility, and rheology are used to quantify thickness, hydrodynamic permeability, and charge density of the stabilizing shell. A collapsed layer at low pH leads to aggregation after addition of salt, while a swollen layer at high pH induces stability. The colloidal interaction potential is deduced from measurements of the high-frequency elastic modulus using torsional resonators. The complex electrosteric forces are shown to be dominated by the excess osmotic pressure created by overlap of the electrosteric layer for particles in contact. The measured moduli G'_∞ can be predicted quantitatively based on a simple model for the osmotic repulsion introduced by Vincent et al. [*J. Colloid Interface Sci.* **1986**, *18*, 261] without adjustable parameters.

Introduction

Polymeric brush coating of colloidal particles is a robust and effective technique for imparting colloidal stability.^{1–4} This so-called “steric stabilization” can be accomplished by a thin emulsifier layer created during classical emulsion polymerization, but generally this effect is achieved by adsorbing^{5,6} or grafting⁷ a polymer onto the surface of the particles. Contrary to pure electrostatic interactions, the steric stabilization is not affected by high salt concentrations, which is important for many applications. *Electrosteric stabilization*, the subject of this work, is created by polyelectrolyte or polyampholyte brushes. For these dispersions, not only the electrostatic stabilization but also the steric stability imparted by the polymer depends on the pH, dielectric properties, and ionic strength of the solvent.⁸ The complex interplay between the electrical properties of the solvent, grafted layer density, and polyelectrolyte properties of the grafted polymer on the stabilization of the colloidal particles makes quantitative investigations of the electrosteric effect both intellectually rich and equally difficult due to the large number of system parameters involved. In what follows, we investigate the properties of a prototype dispersion that is well characterized in order to quantitatively link the dispersion rheology and stability to relatively simple but robust models for the colloidal interaction potential.⁹

The rheology of dispersions of sterically stabilized particles has been studied intensively,^{10–14} and basic colloidal parameters have been deduced from these data. Of interest in quantifying the stabilizing effect of the polymer layer is the interaction potential V . The high-frequency storage modulus G'_∞ is one experimentally accessible quantity that is directly linked to the potential. Theoretical expressions relating G'_∞ and V have been derived for simple liquids,¹⁵ liquid colloidal dispersions,^{16,17} and ordered colloidal systems.^{18,19} Applying these models to predict colloidal dispersion properties led to simple, robust results²⁰ as well as more elaborate theories that include hydrodynamic interactions.^{21,22} Some previous experimental studies of the elastic storage modulus of sterically stabilized particles have used similar theoretical expressions^{23,24} to extract the interaction potential from conventional rheometry. There has been substantially less comparison of theory and measurement for electrosterically stabilized dispersions

* Corresponding author. E-mail: norbert.willenbacher@basf-ag.de.

[†] BASF Aktiengesellschaft.

[‡] University of Delaware.

- (1) Crowl, V. T.; Malati, M. A. *Discuss. Faraday Soc.* **1966**, *42*, 301.
- (2) Smith, T. L.; Bruce, C. A. *J. Colloid Interface Sci.* **1979**, *72*, 13.
- (3) Wong, R.; Hair, M. L.; Croucher, M. D. *J. Imaging Techn.* **1988**, *14*, 129.
- (4) Napper, D. H. *J. Colloid Interface Sci.* **1977**, *58*, 390.
- (5) Greenwood, R.; Luckham, P. F.; Gregory, T. *Colloids Surf., A* **1995**, *98*, 117.
- (6) Sato, T.; Ruch, R. J. *Stabilization of Colloidal Dispersions by Polymer Adsorption*; Marcel Dekker: New York, 1980; Vol. 9.
- (7) Guo, X.; Ballauff, M. *Langmuir* **2000**, *16*, 8719.
- (8) Ortega-Vinuesa, J. L.; Martín-Rodríguez, A.; Hidalgo-Álvarez, R. H. *J. Colloid Interface Sci.* **1996**, *184*, 259.

- (9) Einarson, M. B.; Berg, J. C. *J. Colloid Interface Sci.* **1993**, *155*, 165.
- (10) Frith, W. J.; Strivens, T. A.; Mewis, J. *J. Colloid Interface Sci.* **1990**, *139*, 55.
- (11) Grover, G. S.; Bike, S. G. *Langmuir* **1995**, *11*, 1807.
- (12) Neuhäusler, S.; Richtering, W. *Colloids Surf., A* **1995**, *97*, 39.
- (13) Ponton, A.; Quemada, D.; Lafuma, F.; Neel, O. *Colloids Surf., A* **1996**, *119*, 255.
- (14) Nommensen, P. A.; Duits, M. H. G.; Lopulissa, J. S.; van den Ende, D.; Mellema, J. *Prog. Colloid Polym. Sci.* **1998**, *110*, 144.
- (15) Zwanzig, R.; Mountain, R. D. *J. Chem. Phys.* **1965**, *43*, 4464.
- (16) Bergenholtz, J.; Willenbacher, N.; Wagner, N. J.; Morrison, B.; van den Ende, D.; Mellema, J. *J. Colloid Interface Sci.* **1998**, *202*, 430.
- (17) Wagner, N. J. *J. Colloid Interface Sci.* **1993**, *161*, 169.
- (18) Buscall, R.; Goodwin, J. W.; Hawkins, M. W.; Ottewill, R. H. *J. Chem. Soc., Faraday Trans. 1* **1982**, *78*, 2889.
- (19) Evans, I. D.; Lips, A. *J. Chem. Soc., Faraday Trans.* **1990**, *86*, 3413.
- (20) Deike, I.; Ballauff, M.; Willenbacher, N.; Weiss, A. *J. Rheol.* **2001**, *45*, 709.
- (21) Elliot, S. L.; Russel, W. B. *J. Rheol.* **1998**, *42*, 361.
- (22) Nommensen, P. A.; Duits, M. H. G.; van den Ende, D.; Mellema, J. *Langmuir* **2000**, *16*, 1902.
- (23) Raynaud, L.; Ernst, B.; Vergé, C.; Mewis, J. *J. Colloid Interface Sci.* **1996**, *181*, 11.
- (24) Berli, C. L. A.; Quemada, D. *Langmuir* **2000**, *16*, 7968.

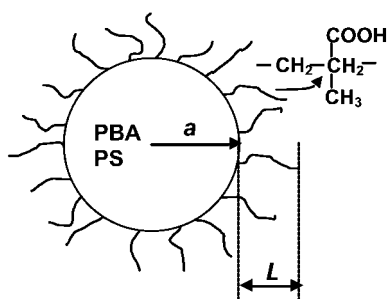


Figure 1. Sketch of the particles studied. Linear chains of poly(methacrylic acid) are grafted on a core of polystyrene–poly(butyl acrylate). The radii a are 47.3 or 54.6 nm; the thicknesses of the polymer layer L vary from 6 to 22 nm. The volume fraction of the stabilizing polymer within the layer varies from 0.04 to 0.15.

The recent development of a series of high-frequency torsional resonators now enables the accurate measurement of the high-frequency elastic and viscous moduli of dispersions of electrosterically stabilized particles.²⁵ In this study, we investigate particles that consist of a polystyrene–poly(butyl acrylate) core with a layer of poly(methacrylic acid) (PMAA) sterically grafted on the surface (Figure 1). This layer is considerably thinner than that examined in the torsional resonator experiments by Deike and co-workers.²⁰ It forms a brushlike structure that exhibits a pronounced dependence on pH because of the acid groups within the stabilizing layer ($pK_a = 5.15$ ²⁶). The pH dependence is linked to a change in the degree of dissociation of the acid groups; as the brush is charged, the structure of the polyelectrolyte brush is also sensitive to the background ionic strength. Further, the amount of polymer within the stabilizing layer is also varied to enhance electrosteric stability. These dispersions are prototypes of modern commercial dispersions used in the coatings industry and, as such, provide a model system for quantifying the effects of solvent properties (pH, ionic strength) and grafted layer density on electrosteric stabilization.

In the following, we present the model dispersions and characterize the extent of the steric layer and the electrosteric stability imparted by the layer at low concentrations. The information obtained from these experiments is used to reduce the broad range of rheological measurements observed at higher concentrations to master curves. A simple model for the electrosteric potential is employed, which connects the measured high-frequency moduli to the polymer concentration and solubility as well as the thickness of the grafted steric layer obtained from independent measurements.

Experimental Section

Synthesis and Purification. Macromonomers were synthesized following Burczyk and co-workers and Janowicz:^{27,28} 836 g of methacrylic acid (BASF) and 39.6 mg of bis(aqua)bis-((difluoroboryl)dimethylglyoximate)cobalt(II) (CoBF, Aldrich) were added to a solution of 77 mg of CoBF and 3.3 g of Azostarter VA 044 (BASF) in 480 g of water. This addition was done slowly and took 1.5 h. The reaction temperature was 55 °C. Polymerization was continued for a further 1.5 h after addition of the methacrylic acid.

Dispersions were prepared by adding an aqueous emulsion of 315 g of styrene (BASF), 385 g of *n*-butylacrylate (BASF), 7.8 g of Dowfax 2A1 (45% w/w in water, Dow Chemicals), and varying amounts of macromonomer (5–8% w/w with respect to total monomer weight) to 21 g of a polystyrene seed (30 nm). The polymerization was initiated by adding a solution of 7 g of sodium persulfate (BASF) in 200 g of water. Feed duration was 4 h, and the reactions were carried out at 85 °C.

The as-synthesized dispersions were dialyzed against deionized water with repeated bath changes until the conductivity of the bath was within 10% of the conductivity of the pure water. An ion-exchange resin (Amberlyst IRN-150, Polysciences) was added to the dispersion for 3 days. Then the dispersion was dialyzed again to reach pH values up to 5 by changing the bath until the desired, constant pH value was achieved; NaOH (Merck) solutions were added directly to the dispersion to achieve pH values higher than 5. Finally, the samples were dialyzed against water baths at the desired salt concentration (NaCl, BASF) and pH. This final dialysis step was combined with a reverse osmosis step (dialysis under pressure) to obtain more concentrated dispersions. The weight fraction of the polymer was determined by drying the samples in a moisture analyzer (Mettler Toledo HR73). Concentration series were prepared by diluting the dispersions with the dialysate.

Measurements. For the dynamic light scattering measurements of the brush swelling with pH, samples were prepared by taking dispersions directly after the ion-exchange step and adjusting them to pH 9 with a NaOH solution. HCl (Fisher Scientific) was added in pH steps of 0.5 until the final pH of 3 was reached. No salt was added for the preparation of this series.

The hydrodynamic size of dispersion particles was measured under dilute conditions using dynamic light scattering (DLS) (Brookhaven, Zeta-PALS). The wavelength used was 677 nm with a scattering angle of 90°. All experiments were done at 20 °C. Critical coagulation concentrations (ccc's) were determined by measuring the development of the DLS autocorrelation function after salt addition during 1 h in 1 min steps. The stability factors were determined from the initial change of the hydrodynamic radius with time²⁹ as well as by shifting the curve of the hydrodynamic radii versus time onto the theoretical master curve.³⁰

Electrophoretic mobilities were measured with a Zeta-PALS instrument (Brookhaven Instruments). Ten measurements (30 cycles per measurement) were made at 20 °C. The resulting mobilities μ_e were converted to the ζ -potential using Henry's equation.³¹

$$\zeta = \frac{3}{2} \frac{\mu_e \mu}{\epsilon \epsilon_0 b}$$

$$b = \frac{1}{2} \left(3 - \frac{9}{\kappa a} + \frac{75}{(\kappa a)^2} - \frac{660}{(\kappa a)^3} \right) \quad (1)$$

where ϵ is the relative dielectric constant of the solvent, ϵ_0 is the permittivity of a vacuum, a is the radius of the particles, κ is the Debye parameter, and μ is the viscosity of the solvent.

The application of Henry's equation to interpret electrophoretic mobilities of electrosterically stabilized dispersions is clearly suspect for "hairy" particles with a soft surface layer. Consequently, Ohshima's model^{32,33} for the mobility of soft spheres was also used to deduce the surface potential from measurements of the electrophoretic mobility at pH 7 for varying salt concentrations.

Low-frequency rheological properties (≤ 100 rad s⁻¹) and zero shear viscosity were obtained from a RFS II rheometer (Rheometrics) using a Couette geometry with an inner diameter of 32 mm and an outer diameter of 34 mm with a cylinder length of 36.4 mm. The measurement cell was thermostated to 20 °C. No

(25) Fritz, G.; Pechhold, W.; Wagner, N. J.; Willenbacher, N. Manuscript in preparation.

(26) Bloys van Treslong, C. J. *Recl. Trav. Chim. Pays-Bas* **1978**, *97*, 13.

(27) Burczyk, A. F.; O'Driscoll, K. F.; Rempal, G. L. *J. Polym. Sci., Polym. Chem.* **1984**, *22*, 3255.

(28) Janowicz, H. U.S. Patent 4,694,054, DuPont, Jan 27, 1986.

(29) Kim, A. Y.; Berg, J. C. *Langmuir* **2000**, *16*, 2101.

(30) Hanus, L. H.; Hartzler, R. U.; Wagner, N. J. *Langmuir* **2001**, *17*, 3136.

(31) Henry, D. C. *Proc. R. Soc. London* **1931**, *A133*, 106.

(32) Ohshima, H.; Kondo, T. *J. Colloid Interface Sci.* **1989**, *130*, 281.

(33) Ohshima, H. *Colloids Surf., A* **1995**, *103*, 249.

significant hysteresis was observed, and low shear plateaus were clearly identifiable.

Torsional Resonators. High-frequency rheology was measured with two torsional resonators supplied by the Institut für dynamische Materialprüfung, Ulm, Germany. The frequencies ω accessible by these instruments are 23 000, 63 000, 119 000, 239 000, and 358 000 rad s⁻¹. Experiments were performed at 20.0 ± 0.1 °C in the surface loading limit.

These resonators are similar to the one used by Bergenholtz and co-workers,¹⁶ and details of their operation and calibration can be found in Fritz et al.²⁵ The shift ΔF of the resonance frequency and the broadening ΔD of the resonance curve of the resonator immersed into the sample relative to the values in air are used to calculate the elastic modulus G' and the loss modulus G'' according to

$$G' = \frac{k}{\rho_s} \left(\left(\frac{\Delta D}{2} \right)^2 - \Delta F^2 \right) + \frac{k}{\rho_s} \frac{2c\Delta D\Delta F}{1 + c^2} + d$$

$$G'' = -\frac{k}{\rho_s} \Delta D\Delta F + \frac{2c}{1 + c^2} \frac{k}{\rho_s} \left(\left(\frac{\Delta D}{2} \right)^2 - \Delta F^2 \right) \quad (2)$$

where k , c , and d are instrumental constants that are determined by measuring a series of Newtonian liquids in the viscosity range from 0.7 to 250 mPa s, while ρ_s is the density of the sample. All three constants have been determined for each frequency.

Theory

In the absence of a steric layer, the interaction potential between colloidal particles is often described in terms of the DLVO potential,^{34,35} which consists of a repulsive electrostatic component V_R and an attractive van der Waals term V_A ,

$$\frac{V_R}{k_B T} = \frac{32\pi\epsilon\epsilon_0 k_B T a}{z^2 e^2} \tanh^2 \left(\frac{ze\psi_d}{4k_B T} \right) \exp(-\kappa H)$$

$$\frac{V_A}{k_B T} = -\frac{A}{6k_B T} \left(\frac{2a^2}{H(4a + H)} + \frac{2a^2}{(2a + H)^2} + \ln \frac{H(4a + H)}{(2a + H)^2} \right) \quad (3)$$

where ψ_d is the diffuse potential, which was assumed to be equal to the ζ -potential,³⁰ k_B is the Boltzmann constant, T is the absolute temperature, z is the electrolyte valence, e is the electron charge, H is the distance between the two particle surfaces, and A is the Hamaker constant. A nonlinear constant potential model for the electrostatic repulsion is used based on the range of parameters explored and previous work.^{30,36}

If the particles are stabilized sterically, two additional terms have to be taken into account:³⁷ An overlap of the polymer brushes for two approaching colloids will result in a local increase in the osmotic pressure due to the increase in the polymer concentration in the overlap region and hence a repulsion V_{Osm} between the particles,³⁸

$$\frac{V_{\text{Osm}}}{k_B T} = 0 \quad 2L \leq H$$

$$\frac{V_{\text{Osm}}}{k_B T} = \frac{4\pi a}{\nu_1} \phi_p^2 \left(\frac{1}{2} - \chi \right) \left(L - \frac{H}{2} \right)^2 \quad L \leq H < 2L$$

$$\frac{V_{\text{Osm}}}{k_B T} = \frac{4\pi a}{\nu_1} \phi_p^2 \left(\frac{1}{2} - \chi \right) L^2 \left(\frac{H}{2L} - \frac{1}{4} - \ln \left(\frac{H}{L} \right) \right) \quad H < L \quad (4)$$

where χ is the Flory–Huggins solvency parameter, ϕ_p is the volume fraction of polymer within the brush layer, L

is the thickness of the brush, and ν_1 is the volume of one solvent molecule. Here, a corresponds to the radius of the core of the particles (i.e., excluding the polyelectrolyte shell). Note that in this simple model the segment density is assumed to be constant inside the brushes and the polymer brushes are assumed not to distort until $H = L$. Compression of the brushes beyond $H = L$ leads to a loss of entropy for the polymers, which gives rise to an entropy elastic repulsion V_{VR} :

$$\frac{V_{\text{VR}}}{k_B T} = 0 \quad L \leq H$$

$$\frac{V_{\text{VR}}}{k_B T} = \left(\frac{2\pi a}{M_w} \phi_p L^2 \rho_p \right) \left(\frac{H}{L} \ln \left(\frac{H(3 - H/L)}{2} \right)^2 - 6 \ln \left(\frac{3 - H/L}{2} \right) + 3 \left(1 + \frac{H}{L} \right) \right) \quad H < L \quad (5)$$

In the above, M_w is the molecular weight of the polymer and ρ_p is its density.

Previous work has assumed that the electrosteric potential can be considered as the linear superposition of these interaction potentials.^{39,40} That is, the resulting total interaction potential V_t can be assumed to be the sum of the components $V_t = V_A + V_R + V_{\text{Osm}} + V_{\text{VR}}$; however, it has been noted that⁹ the steric and the electrostatic double layers are not independent, which leads to a failure of the assumption of additivity. At a minimum, the parameters appearing in the osmotic overlap model for the steric interaction will be a function of the solvent's dielectric constant and ionic strength.

As there is no fully predictive model for the effective colloidal interaction potential for electrosteric stabilization and the superposition of electrostatic and steric components is suspect, we employ a simple ansatz to parametrize our high-frequency rheology measurements in terms of independently verifiable potential parameters. In the following analysis, we will assume that the net effect of the grafted polyelectrolyte in the *swollen* brush on the colloidal interaction parameters can be represented by the simple osmotic pressure model ($V_t = V_{\text{Osm}}$). The main assumption here is that the polyelectrolyte brush provides osmotic stabilization of the colloids. Clearly, the parameters L , ϕ_p , and χ should be considered functions of the pH and ionic strength. However, as we will demonstrate, for the swollen brush over a large range of pH and ionic strengths, good agreement can be achieved if only L , the brush length, is considered to depend on the solvent pH and ionic strength. Further, for the relatively thin and highly stable brushes considered here and for measurements of the linear viscoelastic properties, the brush overlap does not greatly exceed $H < L$ for the concentrations studied, such that significant brush deformation need not be considered.

The high-frequency storage modulus G'_∞ is linked to the interaction potential through an equation derived by Zwanzig and Mountain¹⁵ (neglecting hydrodynamic interactions, see Wagner¹⁷),

$$G'_\infty \frac{a^3}{k_B T} = \frac{3\phi}{4\pi} + \frac{3\phi^2}{40\pi} \int_0^\infty dr g(r) \frac{d}{dr} \left(r^4 \frac{dV_t(r)/k_B T}{dr} \right) \quad (6)$$

where ϕ is the volume fraction of the particles, $g(r)$ is the

(35) Verwey, E. J.; Overbeek, J. T. G. *Theory of the Stability of Lyophobic Colloids*; Elsevier: Amsterdam, 1948.

(36) Russel, W. N.; Saville, D. A.; Schowalter, W. R. *Colloidal Dispersions*; Cambridge University Press: New York, 1989.

(37) Vincent, B.; Edwards, J.; Emmett, S.; Jones, A. *Colloids Surf.* **1986**, *18*, 261.

(34) Derjaguin, B. V.; Landau, L. *Acta Physicochim. USSR* **1941**, *14*, 633.

radial distribution function that describes positional correlations among particles in the equilibrium fluid, and r is the distance from the center of the particle. Note that $g(r)$ depends on the interaction potential V_i and particle concentration.

In the following, a first-order perturbation about a hard-sphere (HS) state will be consistently applied to provide an analytic connection between the elastic modulus and the osmotic pressure overlap potential. For liquid dispersions with steep, short-range repulsive interactions, eq 6 can be approximated according to Bergholtz and co-workers¹⁶ by

$$\frac{G_{\infty} a^3}{k_B T} = \frac{3\phi}{4\pi} + \frac{3\phi^2}{40\pi} \left(\frac{D_{\text{eff}}}{a} \right)^4 g_{\text{HS}}(D_{\text{eff}}, \phi_{\text{eff}}) F(D_{\text{eff}})$$

$$F(D_{\text{eff}}) = - \frac{\partial V_t}{\partial r} \frac{a}{k_B T} \Big|_{r=D_{\text{eff}}} \quad (7)$$

The true $g(r)$ is approximated by the pair distribution function $g_{\text{HS}}(r)$ of an effective hard-sphere suspension with particles of diameter D_{eff} , and only interactions between nearest neighbors are taken into account. The force F acting between the particles is used in eq 7 in a dimensionless form. This method by Bergholtz and co-workers uses a hard-sphere approximation for the liquid structure and does not assume a crystal structure as done by others.¹⁸ Therefore, the distance between nearest-neighbor particles is determined by their effective diameter and not by the spacing of a presumed crystal lattice.

For stable dispersions with swollen polyelectrolyte brushes, the hydrodynamic radius, as determined from the divergence of the zero shear viscosity and the DLS measurements, gives the core radius a and the layer thickness L . Then, using the simplified osmotic pressure model for the net interaction potential under conditions of small brush deformation, eq 7 can be written explicitly as

$$\frac{G_{\infty} a^3}{k_B T} \approx \frac{3\phi_{\text{core}}^2 \phi_P^2 a^2}{10\nu_1} \left(\frac{D_{\text{eff}}}{a} \right)^4 \left(\frac{1}{2} - \chi \right) \left(L + a - \frac{D_{\text{eff}}}{2} \right) g_{\text{HS}}(D_{\text{eff}}, \phi_{\text{eff}}) \quad (8)$$

where ϕ_{core} is the volume fraction of the cores of the particles. The term $3\phi/4\pi$ in eq 7 is the single-particle contribution to G_{∞} , which can generally be neglected for interacting systems.

The effective hard-sphere diameter D_{eff} is calculated from the Barker–Henderson⁴¹ first-order perturbation theory applied to the simplified osmotic pressure overlap potential as

$$D_{\text{eff}} = 2a + \int_0^{2L} \left(1 - \exp \left[- \frac{4\pi a}{\nu_1} \phi P^2 \left(\frac{1}{2} - \chi \right) \left(L - \frac{H}{2} \right)^2 \right] \right) dH \quad (9)$$

The radial distribution function at contact can be calculated by means of the Carnahan–Starling expression,⁴²

$$g_{\text{HS}}(D_{\text{eff}}, \phi_{\text{eff}}) = \frac{1 - \phi_{\text{eff}}/2}{(1 - \phi_{\text{eff}})^3} \quad (10)$$

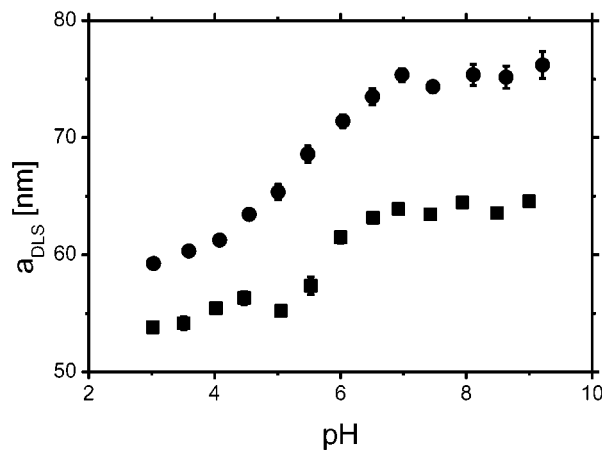


Figure 2. Hydrodynamic radius variation with pH. The dissociation of the acid groups in the PMAA layer leads to a swelling of the shell. ■, 5% PMAA; ●, 8% PMAA.

Here, we use the liquid structure beyond the HS phase transition ($\phi = 0.5$) as our interaction potential is soft and there is no evidence for crystallization of the samples in the range of concentrations reported here.

For the conditions assumed here, eq 8 can be rearranged to yield

$$\frac{G_{\infty} D_{\text{eff}}^2 2a}{k_B T} \approx \frac{3 \times 2^6}{5} \phi_{\text{eff}}^2 \phi_P^2 \frac{a^3}{\nu_1} \left(\frac{1}{2} - \chi \right) \left(\frac{L}{a} + 1 - \frac{D_{\text{eff}}}{2a} \right) \frac{1 - \phi_{\text{eff}}/2}{(1 - \phi_{\text{eff}})^3} \quad (11)$$

Notice that the dimensionless modulus $G_{\infty} D_{\text{eff}}^2 2a / k_B T$ is a function of the effective hard-sphere volume fraction ϕ_{eff} , the volume fraction of polymer in the stabilizing layer ϕ_P , the Flory–Huggins parameter χ , the ratio of layer thickness to core radius L/a , the ratio of the effective hard-sphere diameter to the core diameter D_{eff}/a , and the ratio a^3/ν_1 . The parameters ϕ_P and χ can be assumed to be relatively constant. If the ratios L/a , a^3/ν_1 , and $D_{\text{eff}}/2a$ do not vary significantly, the only strong dependence of $G_{\infty} D_{\text{eff}}^2 2a / k_B T$ is on the effective hard-sphere volume fraction. Thus, a master curve is expected to hold approximately for a given particle size and stabilizer when $G_{\infty} D_{\text{eff}}^2 2a / k_B T$ is plotted against the effective hard-sphere volume fraction. The weak variation of the other parameters is expected to introduce some broadening. This behavior contrasts with that of simple hard-sphere colloids, where the simple scaling $G_{\infty} a^3 / k_B T$ leads to a master curve as a function of volume fraction.⁴³

Results and Discussion

Dynamic Light Scattering and Low Shear Viscometry. The acid groups in the sterically stabilizing layer result in a pH dependence of the polymer brush properties. Deprotonation of these groups leads to an enhanced repulsion within and between the polymer chains, which results in a swelling of the PMAA layer. This in consequence gives rise to an increase of the hydrodynamic radius measured by DLS (Figure 2). This effect of the degree of ionization on the conformation of PMAA and thereby on the size of the particles is similar to the swelling of curved

(40) Likos, C. N.; Vaynberg, K. A.; Löwen, H.; Wagner, N. J. *Langmuir* **2000**, *16*, 4100.

(41) Barker, J. A.; Henderson, D. *J. Chem. Phys.* **1967**, *47*, 4714.

(42) Carnahan, N. F.; Starling, K. E. *J. Chem. Phys.* **1969**, *51*, 635.

(43) Lionberger, R. A.; Russel, W. B. *J. Rheol.* **1994**, *38*, 1885.

(38) Fischer, E. *Kolloid-Z.* **1958**, *160*, 120.

(39) Kamiyama, Y.; Israelachvili, J. *Macromolecules* **1992**, *25*, 5081.

PAA brushes⁷ and planar PMAA brushes⁴⁴ and to the dramatic conformational changes observed for free PMAA in solution upon neutralization.⁴⁵ The swelling with pH for free polymer in solution can be attributed to a conformational change from a compact, hypercoiled, hydrophobically associated, impermeable coil to an extended, swollen state. The similarity between the pH dependence of the thickness of the grafted brush and the behavior of the polymer free in solution suggests that qualitatively the same behavior is observed for the grafted PMAA despite the differences in ion distribution and therefore in the degree of swelling.

The increase of the hydrodynamic radius with pH observed in dilute solution is also observed for the effective hard-sphere particle size obtained from the zero shear viscosity data. This experimental quantity allows one to link the known mass fractions to the effective hard-sphere volume fractions by mapping the measured zero shear viscosity data to a hard-sphere dispersion described by the phenomenological Quemada equation⁴⁶

$$\frac{\eta_0}{\mu} = \left(1 - \frac{\phi_{\text{eff}}}{\phi_{\text{max}}}\right)^{-2} \quad (12)$$

The maximum packing fraction ϕ_{max} , where the zero shear viscosity diverges, is assumed to be at the HS glass transition,^{16,47–50} which is taken to be 0.58.^{51,52}

The exponent -2 in eq 12 is correct in the limit of $\phi_{\text{eff}} \rightarrow \phi_{\text{max}}$, while the expression is only an approximation at lower volume fractions.⁵³ Therefore, the transformation of mass fraction into effective volume fraction has to be based on high volume fractions. First, the data sets with relative zero shear viscosities of about 15 or higher (corresponding to $\phi_{\text{eff}} > 0.43$) were shifted onto the curve given by Quemada's expression by multiplying the mass fraction with a factor f . The lower concentrations of the concentration series of these samples were shifted by the same factors f to define a first master curve. Since some samples could not be prepared at concentrations to yield relative zero shear viscosities greater than 15, these samples were shifted onto this first master curve and not onto the curve obtained from Quemada's expression. Again, only one factor f was used for each concentration series. As shown, all the data collapse onto a master curve with a single shift factor independent of concentration for each sample. That this master curve is not fully described by the Quemada equation at low concentrations is not unexpected nor important for the following analysis.

The factors f that are used to scale the mass fractions of the sample to effective volume fractions relate the layer thickness to the core radius of the particles. Geometric considerations yield

$$f = \frac{\phi_{\text{eff}}}{\rho w \phi_{\text{core}}} = \frac{1}{\rho w} \left(1 + \frac{L}{a}\right)^3 \quad (13)$$

where ρ is the density of the particle core (1.05 g/mL), ϕ_{core} is the volume fraction of the particle core, and w is a factor

Table 1. Particle Size and Layer Properties of Lattices Stabilized by 5% and 8% PMAA at Different pH Values and Salt Concentrations^a

sample	a_{DLS} [nm]	$a_{\eta 0}$ [nm]	f	L [nm]	ϕ_{P}
5%, pH 4, 10 mM	53.3*	53.3	1.30	6.0	0.115
5%, pH 5, 105 mM	60.4	54.0	1.35	6.7	0.102
5%, pH 5, 500 mM	60.2	55.4	1.45	8.1	0.083
5%, pH 7, 100 mM	68.3	63.6	2.21	16.3	0.034
5%, pH 7, 500 mM	64.2	58.9	1.75	11.6	0.054
5%, pH 9, 260 mM	66.6	62.3	2.07	15.0	0.039
5%, pH 9, 500 mM	63.8	58.9	1.75	11.6	0.054
8%, pH 4, 10 mM	67.5*	67.5	1.66	12.8	0.091
8%, pH 4, 100 mM	68.4	62.8	1.34	8.2	0.153
8%, pH 5, 8 mM	73.3	67.3	1.65	12.7	0.092
8%, pH 5, 500 mM	73.9	64.5	1.45	9.8	0.124
8%, pH 7, 100 mM	75.9	76.9	2.46	22.3	0.045
8%, pH 7, 500 mM	74.0	70.4	1.89	15.8	0.070
8%, pH 9, 260 mM	74.4	75.5	2.33	20.9	0.049
8%, pH 9, 500 mM	72.7	72.5	2.07	17.9	0.060

^a Hydrodynamic radii are shown according to DLS (a_{DLS}) and zero shear viscosity ($a_{\eta 0}$) data. The pH 4, 10 mM samples (marked with an asterisk) have been used to determine the core particle radii. The factor to convert mass fraction into volume fraction as determined by zero shear viscosity is f , the thickness of the polymer brush is L , and ϕ_{P} gives the volume fraction of PMAA within the steric stabilization layer.

that takes the known mass fraction of the steric layer into account (1.05 for 5% PMAA, 1.08 for 8%). Using the measured hydrodynamic radii and assuming $a_{\text{DLS}} = a + L$, the core radius and the layer thickness can be calculated from the measurements of the zero shear viscosity and the dilute hydrodynamic radius. It is also reasonable to assume that the core radius is independent of pH and ionic strength, while L should vary with pH and ionic strength. On the other hand, the hydrodynamic radius determined by DLS is dominated by the longest chains in the outer region of the brush,^{7,54} which is not necessarily the same brush thickness as measured by viscometry. Therefore, we used the data at pH 4 and 10 mmol/L ionic strength to calculate the core radii for the 5% and 8% PMAA dispersions. At this low ionic strength, the dispersions remain stable. A pH of 4 is below the PMAA transition from collapsed to swollen shell. This ensures that the steric layer is mostly collapsed and that the number of chains projecting into the water is minimized (note that $f > \rho^{-1}$ and therefore the brush is not completely collapsed). In this manner, the core radius of the 5% PMAA dispersion was found to be 47.3 nm while the 8% PMAA dispersion has a radius of 54.6 nm. This compares favorably with the value of 48.8 nm for the core particle size estimated from the chemical synthesis conditions.

Given this constant core radius, the effective hard-sphere radii can be calculated from the effective hard-sphere volume fraction and the constant core radius (Table 1). As seen in Table 1, the effective hard-sphere radius determined from the shear viscosity is generally less than the hydrodynamic radius determined from DLS in dilute solution under the same solvent conditions, as expected. The deviation is consistent with an open brush with a finite hydrodynamic permeability. Further, as the viscometric value of the radius is determined at much higher

(44) Biesalski, M.; R  he, J.; Johannesmann, D. *J. Chem. Phys.* **1999**, *111*, 7029.

(45) Eisenberg, H.; Pouyet, J. *J. Polym. Sci.* **1954**, *13*, 85.

(46) Quemada, D. *Rheol. Acta* **1977**, *16*, 82.

(47) Meeker, S. P.; Poon, W. C. K.; Pusey, P. N. *Phys. Rev. E* **1997**, *55*, 5718.

(48) Fritz, G.; Maranzano, B. J.; Wagner, N. J.; Willenbacher, N. *J. Non-Newtonian Fluid Mech.*, in press.

(49) Bergenholtz, J.; Horn, F. M.; Richtering, W.; Willenbacher, N.; Wagner, N. J. *Phys. Rev. E* **1998**, *58*, 4088.

(50) Horn, F. M.; Richtering, W.; Bergenholtz, J.; Willenbacher, N.; Wagner, N. J. *J. Colloid Interface Sci.* **2000**, *225*, 166.

(51) van Megen, W.; Underwood, S. M. *Phys. Rev. E* **1994**, *49*, 4206.

(52) Phan, S.-E.; Russel, W. B.; Cheng, Z. D.; Zhu, J. X.; Chaikin, P. M.; Dunsmaier, J. H.; Ottewill, R. H. *Phys. Rev. E* **1996**, *54*, 6633.

(53) Brady, J. F. *J. Chem. Phys.* **1993**, *99*, 567.

(54) Lyatskaya, Y. V.; Leermakers, F. A. M.; Fleer, G. J.; Zhulina, E. B.; Birshtein, T. M. *Macromolecules* **1995**, *28*, 3562.

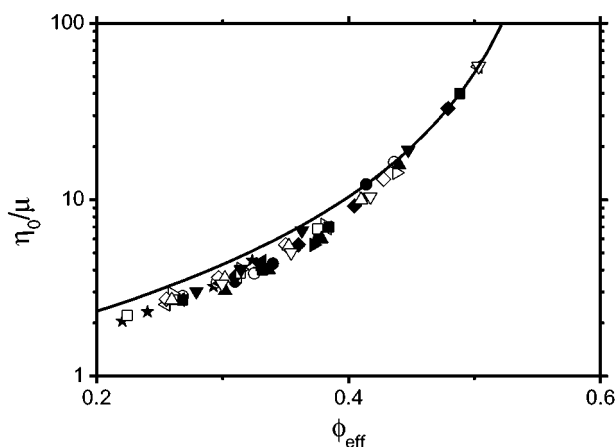


Figure 3. The relative zero shear viscosity plotted against the scaled effective volume fraction ϕ_{eff} . pH 4: 5%, 10 mM (★); 8%, 10 mM (●); 8%, 100 mM (○). pH 5: 5%, 105 mM (left-pointing solid triangle); 8%, 8 mM (right-pointing solid triangle); 5%, 500 mM (left-pointing open triangle); 8%, 500 mM (right-pointing open triangle). pH 7: 5%, 100 mM (■); 8%, 100 mM (◆); 5%, 500 mM (□); 8%, 500 mM (◇). pH 9: 5%, 260 mM (▲); 8%, 260 mM (▼); 5%, 500 mM (△); 8%, 500 mM (▽). The data are scaled to the Quemada expression (solid line, eq 12) at high concentrations.

concentrations ($\phi_{\text{eff}} \approx 0.5$ instead of 0.5×10^{-5}), some compression of the polyelectrolyte brush could also be expected.

These values can also be used to calculate a mean layer thickness L for all samples below and above the pH value where the polymer shell swells. The 5% PMAA sample has a typical thickness of the swollen brush (from the pH 7 and pH 9 data) of 14 nm, while the shell of the 8% sample is 19 nm thick. From these values, the amount of macromonomers (known from synthesis), and the core particle sizes, it is possible to calculate the average volume fraction ϕ_p of polymer in the swollen brush to be 4.4% for the 5% PMAA dispersion and 5.4% for the 8% sample. Thus, each grafted polymer occupies a volume of about 250 nm³ per polymer chain in the case of the 5% PMAA sample and about 200 nm³ for the 8% PMAA sample. For reference, the volume in solution of one PMAA chain of a molecular weight of 7000 g/mol is about 460 nm³. Therefore, the polymer concentration within the shell corresponds to about 1.8 (5% PMAA) and 2.3 (8% PMAA) times the overlap concentration c^* .

Electrokinetics. The charge of the polyelectrolyte shell gives rise to an electrophoretic mobility of the dispersion particles. In the case of pH 4 where the brush is collapsed, the mobility can be converted into the ζ -potential, which is found to be −34 mV for the 5% PMAA sample and −33 mV for the 8% PMAA sample. At higher pH values, the mobility depends on salt concentration, which can be described by Ohshima's model for the mobility of charged soft spheres^{32,33} (Figure 4). The charge density within the layer and the rigidity parameter λ were used as free parameters to fit the model to the experimental data (λ is proportional to the square root of the frictional coefficient;⁵⁵ an increase in λ corresponds to a more rigid layer). Note that the model does not take into account the dependence of layer thickness on salt concentration. At pH 7, the 5% PMAA particles were found to have a charge density of 37 mol m^{−3} and a λ parameter of 0.5 nm^{−1} while the 8% PMAA particles have a charge density of 60 mol m^{−3} and a rigidity parameter of 0.8 nm^{−1}. The charge

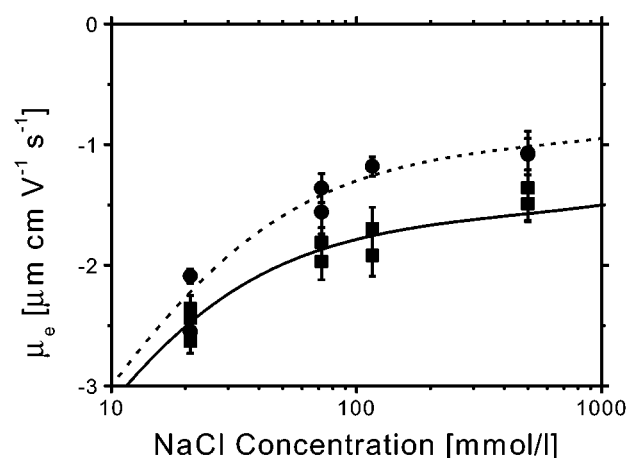


Figure 4. Electrophoretic mobility of the particles (0.03% (w/w)) at pH 7 as a function of salt concentration. ■, 5% PMAA; ●, 8% PMAA. The lines represent the approximation by the Ohshima model for the 5% (solid line) and 8% (dashed line) PMAA dispersions. The model gives charge densities of 37 mol m^{−3} (5%) and 60 mol m^{−3} (8%), while the stiffness parameter λ is 0.5 nm^{−1} for the 5% sample and 0.8 nm^{−1} for the 8% sample.

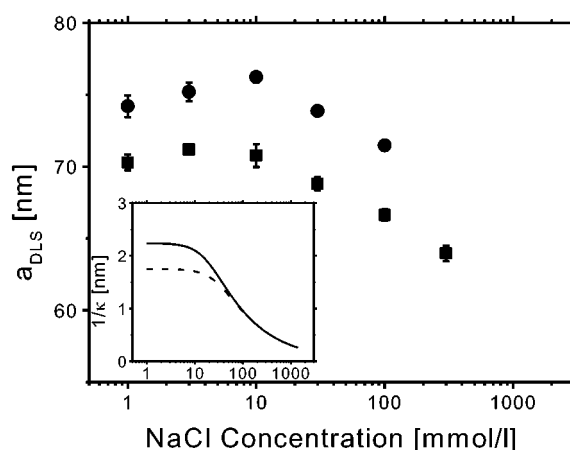


Figure 5. Dependence of hydrodynamic radii a_{DLS} on salt concentration at pH 7. The screening of the charges in the polyelectrolyte brushes leads to a decrease in layer thickness. ■, 5% PMAA; ●, 8% PMAA. The Debye screening length $1/\kappa$ within the polymer brush according to the Ohshima model is plotted for comparison. Solid line, 5% PMAA; dashed line, 8% PMAA. The particle concentration is 0.03% (w/w).

densities of both samples are about 1 order of magnitude below the values expected from stoichiometric calculations, which suggests substantial charge regulation. On the other hand, the ratio of the charge densities of the 8% brush to the 5% brush is 1.6, which is reasonably close to the ratio (1.3) of the polymer concentrations within the layer. The higher λ parameter of the 8% PMAA samples seems to reflect the higher volume fraction of polymer within the shell, which leads to greater rigidity. The consistency of the electrophoretic mobility, DLS, and viscometric measurements with the composition of the particles supports the validity of the parameters extracted and reported in Table 1.

The PMAA shell consists of a swollen polyelectrolyte at high pH values. Therefore, an increase of the ionic strength leads to enhanced screening of the charges within the layer, which leads to a decrease in layer thickness (Figure 5). As stated above, this feature is not included in the Ohshima model. The dependence of the particle size on salt concentration, however, shows a behavior that is correlated to the electrostatic screening length, as char-

(55) Larsson, A.; Rasmussen, M.; Ohshima, H. *Carbohydr. Res.* **1999**, *317*, 223.

acterized by the Debye length within the stabilizing shell. Using the parameters derived from the Ohshima model, the calculation of the Debye length takes into account the dissociated counterions from the charge density within the layer, which contribute about 10 mmol/L to the ionic strength at pH 7. Addition of salt in excess of this background value leads to a decrease in Debye length. The added salt concentration at which the Debye length begins to decrease corresponds to the observed decrease in the hydrodynamic radius of the dispersion. The consistency of this calculation with experimental observation validates the quantification of the layer charge density using the Ohshima model and highlights the significance of changes in solvent ionic strength on the brush properties.

Stability at Low pH: Collapsed Surface Layer. For collapsed brushes at pH 4–5, the electrostatic potential can be screened by adding salt and at high ionic strength a loss of stability is observed.⁵⁶ This has been characterized quantitatively by determination of the so-called stability factor W , which is given as the ratio of the rate constants for rapid and slow aggregation. W is related to the particle interaction potential according to³⁶

$$W = 2a \int_0^\infty \frac{\exp(V_t(H)/k_B T)}{(H + 2a)^2 G(H)} dH \quad (14)$$

where $G(H)$ is a hydrodynamic function, which has to be calculated numerically.⁵⁷

Quantitative analysis of the stability factors using the initial slope of the hydrodynamic radius versus time curves yields critical coagulation concentrations of 1.22 mol/L for 5% PMAA and 2.38 mol/L for 8% PMAA dispersions at pH = 4. If the DLS data are analyzed according to the master curve method by Hanus and co-workers,³⁰ critical coagulation concentrations of 1.34 and 2.29 mol/L are obtained (Figure 6).⁵⁸

The observed aggregation requires that the particles can come close enough that the attractive potential becomes dominant. However, even at pH 4 and 10 mM NaCl, the brush layer thickness reported in Table 1 would keep the particle cores separated enough to prevent aggregation. Therefore, either some poor solvency must be invoked to provide an additional attractive potential or some estimate of the additional dispersion forces arising from the layer must be made. As a first estimate of the latter, we assume a totally collapsed layer with a density equal to that of the core at these high salt concentrations, which corresponds to a core that has been increased by 5% or 8% in volume. Thus, the radius of the compact part of the particles increases by 0.8 nm for the 5% PMAA and 1.4 nm for the 8% PMAA particles. The standard Derjaguin–Landau–Verwey–Overbeek (DLVO) potential is then presumed to start from this radius. Theoretical calculations of the stability factors W show that such electrostatically stabilized particles should have their ccc at about 0.7–0.8 mol/L NaCl (Figure 6, dotted line); that is, this first approximation overestimates the loss in stability upon collapse of the brush.

(56) At pH greater than or equal to 7, no aggregation occurs up to salt concentrations of 3.5 mol/L NaCl.

(57) Batchelor, G. K. *J. Fluid Mech.* **1976**, 74, 1.

(58) This master curve technique also yields an estimation of the fractal dimension of the aggregates, which is found to be 1.41 ± 0.08 . This corresponds to a very loose structure of the aggregates since theoretical calculations [Russel et al. *Colloidal Dispersions* 1989] and experiments [Hanus et al. *Langmuir* **2001**, 17, 3136] find fractal dimensions of 1.8 and 1.86, respectively, for cluster–cluster aggregation, which is typically found for dispersions of electrostatically stabilized particles.

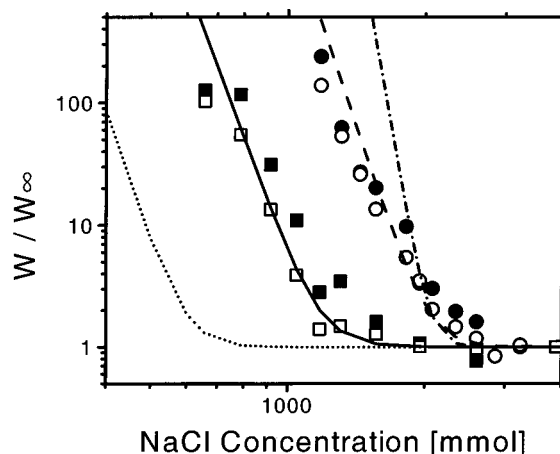


Figure 6. Stability factors of samples at pH 4 for various salt concentrations: 5% PMAA (■), 8% PMAA (●). Solid symbols correspond to values determined from shifting the development of the hydrodynamic radii onto the theoretical master curve, while open symbols are stability factors determined from the initial change in radius. Theoretical values calculated from the DLVO interaction potential using eq 14 with the effective Hamaker constant for 5% (solid line) and 8% PMAA (dashed line). The dotted line is the theoretical stability factor of the 8% PMAA dispersion without adjusting the Hamaker constant. The dashed–dotted line corresponds to the theoretical stability factor of the 8% PMAA dispersion without changing the Hamaker constant but with an increased ζ -potential of -46 mV.

One possibility to reduce this obvious disagreement with experiment is to assume a weaker effective Hamaker constant due to the core–shell structure of the particles. We have used the Hamaker constant of poly(methyl methacrylate)³⁰ (7.56×10^{-21} J) to approximate the constant for our particle cores in water. This constant is also comparable to 9×10^{-21} J, the value reported for polystyrene,^{8,59} the component that contributes 46% of the mass of the particle cores. Reducing the Hamaker constant to effective values of $A_{\text{eff}} = 5.6 \times 10^{-21}$ J for the 5% PMAA dispersion and $A_{\text{eff}} = 4.0 \times 10^{-21}$ J for the 8% PMAA dispersion approximates the experimentally observed stabilities (Figure 6, solid and dashed lines). Alternatively, increasing the strength of the electrostatic potential and leaving the Hamaker constant unchanged leads to high ζ -potentials of -38 and -46 mV for the 5% and 8% PMAA particles and an overestimate of the dependence of W on electrolyte concentration (Figure 6, dashed–dotted line). Finally, two other possible explanations for the electrolyte dependence of the stability ratio can be considered: In the collapsed state, there may be some residual steric repulsion due to “roughness” of the collapsed layer. Adding a few nanometers of surface roughness as a steric stabilization to the original DLVO potential can yield results in quantitative agreement with the measurements, but with the additional fit parameters of the strength and range of the steric repulsion (e.g., an additional contribution of $\phi_p = 0.1$ can explain the behavior according to eqs 4 and 5 with a 1.3 nm layer for the 5% PMAA sample and a 1.6 nm layer for the 8% sample). Further, as the pH is lowered and salt is added, poorer solvent conditions (i.e., $\chi > 1/2$) could lead to an attraction of the polymers in the layer leading to aggregation.⁶⁰ Thus, although we can fit the observed stability ratios with the simple DLVO potential and a reduced Hamaker constant,

(59) Prieve, D. C.; Russel, W. B. *J. Colloid Interface Sci.* **1988**, 125, 1.

(60) Napper, D. H. *Polymeric Stabilization of Colloidal Dispersions*; Academic Press: New York, 1983.

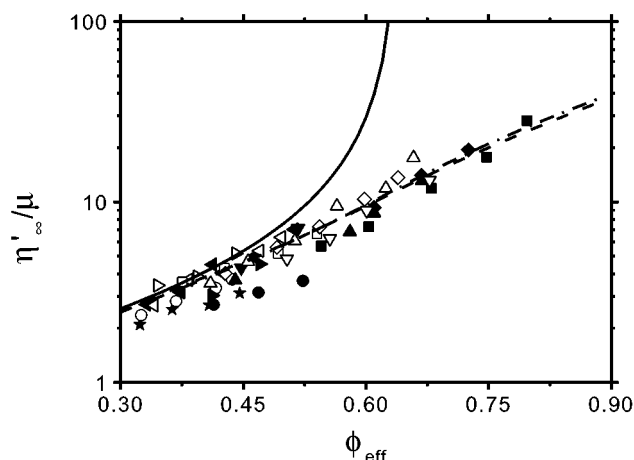


Figure 7. High-frequency viscosity ($358\,000\text{ rad s}^{-1}$). pH 4: 5%, 10 mM (★); 8%, 10 mM (●); 8%, 100 mM (○). pH 5: 5%, 105 mM (left-pointing solid triangle); 8%, 8 mM (right-pointing solid triangle); 5%, 500 mM (left-pointing open triangle); 8%, 500 mM (right-pointing open triangle). pH 7: 5%, 100 mM (■); 8%, 100 mM (◆); 5%, 500 mM (□); 8%, 500 mM (◇). pH 9: 5%, 260 mM (▲); 8%, 260 mM (▼); 5%, 500 mM (△); 8%, 500 mM (▽). Lionberger–Russel expression for hard spheres (solid line, eq 15) and Potanin and Russel theory for particles with grafted polymer layers: 5% PMAA, $a/L = 3.47$, $L/\delta = 5.7$ (dashed line); 8% PMAA, $a/L = 2.84$, $L/\delta = 6.6$ (dashed–dotted line).

further experiments would be required to resolve the mechanism of loss of stability for these electrosterically stabilized dispersions at low pH.

Stability at High pH: High-Frequency Rheology; Swollen Surface Layer. High-frequency rheology measurements were carried out on the stable dispersions as a function of dispersion concentration, solvent pH and ionic strength, and amount of PMAA stabilizer. The moduli measured at the highest frequency ($358 \times 10^3\text{ rad s}^{-1}$) are taken here as the limiting values G'_∞ and will be discussed in the following section.

Although the absolute measurements of the high-frequency viscosity varied over orders of magnitude with changes in these parameters, all of the measured data could be readily scaled onto a master curve if plotted against the effective volume fraction as determined by the zero shear viscosity (Figure 7). The reduction of the high-frequency viscosity, which is a purely hydrodynamic quantity, to a master curve when reduced by an effective volume fraction determined from the maximum packing fraction for the zero shear viscosity is not expected a priori, as the latter explicitly includes interparticle forces. Comparing these data with the semiempirical expression that has been proposed by Lionberger and Russel for a hard-sphere dispersion,⁴³

$$\frac{\eta'_\infty}{\mu} = \frac{1 + \frac{3}{2}\phi(1 + \phi - 0.189\phi^2)}{1 - \phi(1 + \phi - 0.189\phi^2)} \quad (15)$$

shows that the soft-sphere results are in general below the hard-sphere data. This difference increases with the volume fraction. It should also be noted that the hard-sphere expression diverges at $\phi_{\text{max}} = 0.64$ while the soft spheres can reach effective volume fractions that are considerably higher and even exceed the limit of $\phi_{\text{max}} = 0.74$ for cubic close packing. This is due to the fact that the polymer brushes can compress and interpenetrate. The deviations from HS behavior at lower volume fractions are evidence for the hydrodynamic permeability of the polyelectrolyte brushes, as discussed by Elliot and Rus-

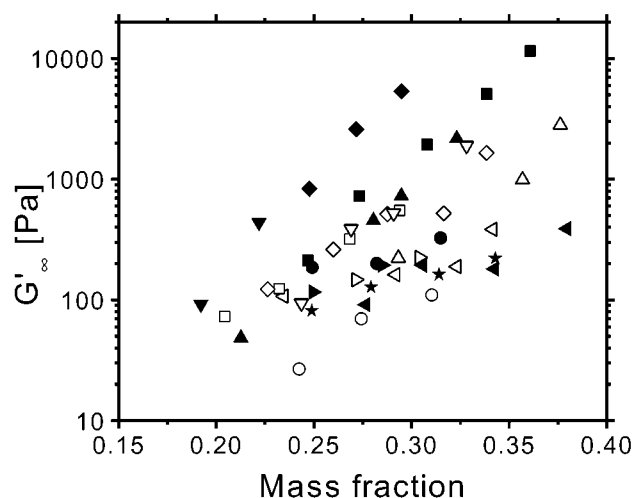


Figure 8. High-frequency modulus ($358\,000\text{ rad s}^{-1}$). pH 4: 5%, 10 mM (★); 8%, 10 mM (●); 8%, 100 mM (○). pH 5: 5%, 105 mM (left-pointing solid triangle); 8%, 8 mM (right-pointing solid triangle); 5%, 500 mM (left-pointing open triangle); 8%, 500 mM (right-pointing open triangle). pH 7: 5%, 100 mM (■); 8%, 100 mM (◆); 5%, 500 mM (□); 8%, 500 mM (◇). pH 9: 5%, 260 mM (▲); 8%, 260 mM (▼); 5%, 500 mM (△); 8%, 500 mM (▽).

sel.²¹ This hydrodynamic permeability can be described by the theory by Potanin and Russel⁶¹ for η'_∞/μ (using the equations corrected for typographical errors given by Elliot and Russel in the appendix of their paper to calculate the hydrodynamic force and the expression for the viscosity of concentrated suspensions by Frankel and Acrivos⁶²). Calculations were done for typical a/L ratios of the pH 7 and 9 samples (3.55 for 5% PMAA and 2.89 for 8% PMAA). Fitting the theory to our data gives $\delta = 2.6 \pm 0.2\text{ nm}$ for 5% PMAA and $2.8 \pm 0.2\text{ nm}$ for 8% PMAA, where δ can be interpreted as a characteristic “mesh size”.⁶¹

The high-frequency modulus is plotted versus mass fraction of the polymer particles in Figure 8. The modulus increases steeply with increasing amount of grafted polymer but also varies strongly with pH, ionic strength, and amount of grafted polymer. Nevertheless, the data collapse surprisingly well onto a master curve when the scaling suggested by the osmotic brush overlap model is applied (see eq 11). This is demonstrated in parts a and b of Figure 9 for the systems with 5% and 8% grafted polymer, respectively.⁶³ The observed scaling behavior suggests that osmotic interactions dominate the high-frequency rheology of the system investigated here.

For reference, the hard-sphere curve is given for both systems in Figure 9. The data lie above the hard-sphere line at low volume fractions and do not diverge as predicted for hard spheres. These deviations reveal the nature of the electrosteric layer. At high concentrations, the softness of the electrosteric potential leads to interpenetration of the layer, rather than the divergence predicted for hard spheres. Published calculations²¹ have shown that increasing hydrodynamic porosity increases G' at lower concentrations, which is also consistent with the experimental observations. Thus, the deviations from HS behavior are expected for interpenetrable, porous stabilizing layers.

To predict G'_∞ quantitatively, we first estimate the mean particle surface separation H from eq 16:

$$2a \left(\frac{a+L}{a} \sqrt[3]{\frac{\phi_{\text{core,max}}}{\phi_{\text{eff}}}} - 1 \right) = H \quad (16)$$

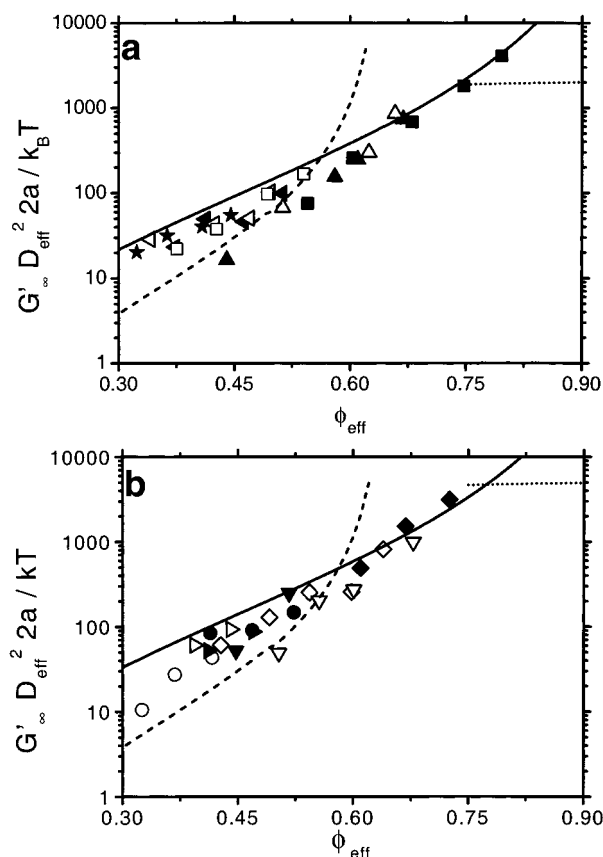


Figure 9. Dimensionless high-frequency storage modulus. (a) 5% data. pH 4: 10 mM (★). pH 5: 105 mM (left-pointing solid triangle); 500 mM (left-pointing open triangle). pH 7: 100 mM (■); 500 mM (□). pH 9: 260 mM (▲); 500 mM (△). (b) 8% data. pH 4: 10 mM (●); 100 mM (○). pH 5: 8 mM (right-pointing solid triangle); 500 mM (right-pointing open triangle). pH 7: 100 mM (◆); 500 mM (◇). pH 9: 260 mM (▼); 500 mM (▽). Solid lines: model for sterically stabilized dispersions (5% PMAA: $a = 47.3$ nm, $L = 13.6$ nm, $\phi_p = 0.044$, $D_{\text{eff}} = 119.5$ nm; 8% PMAA: $a = 54.6$ nm, $L = 19.2$ nm, $\phi_p = 0.054$, $D_{\text{eff}} = 145.9$ nm). Dashed lines: Lionberger–Russel theory for hard spheres. Dotted lines: Buscall theory for face-centered cubic lattice. The scaling of the ordinate is approximated by $2(a + L) \approx D_{\text{eff}}$ to exclude influence of the assumed interaction potential on the scaling.

In the above, $\phi_{\text{core,max}} = 0.58$ is the maximum packing fraction of the particle cores. Calculations show that the surface-to-surface separation H is larger than the individual brush thickness even for the highest effective volume fractions; thus we can neglect the elastic contributions to the interaction potential. The electrostatic interaction potential can be estimated from the electrokinetic data discussed above. An estimation of the contributions to the total interaction potential in the vicinity of D_{eff} is shown in Figure 10. The osmotic contribution to V_t is the dominant term. Thus G_{∞} can be calculated according to eq 11; the potential arises primarily from the osmotic pressure induced by the overlapping polymer brushes.

The simple model introduced above uses no free parameters. The Flory–Huggins parameter is taken to be 0.485;⁶⁴ the core radius and the volume of the solvent

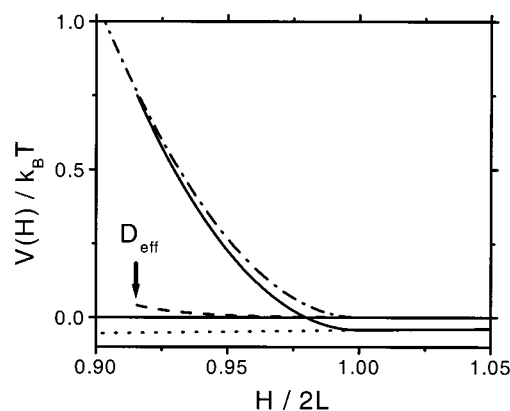


Figure 10. The total interaction potential V_t (solid line) of 5% PMAA close to the effective particle diameter. The contributions are V_{Osm} (dashed–dotted line, eq 4), V_A (dotted line, eq 3), and V_R (dashed line). V_R has been estimated from eq 3, by setting ψ_d equal to the surface potential obtained from the electrophoretic mobility at D_{eff} . The polymer chain deformation does not influence the potential at $H/2L > 1/2$. The arrow marks D_{eff} (eq 9).

molecules are known independently. The solid lines in Figure 9a,b are calculated using averaged values for layer thickness L and polymer concentration ϕ_p from the data sets obtained at pH 7 and 9, when the steric layer is fully developed. The theoretical curves agree well with the experimental data. Therefore, this simplified, “practical” osmotic pressure overlap model is an accurate representation of the interaction potential of the electrosteric brush. We note that average parameter values have been used for ϕ_p , L/a , and $D_{\text{eff}}/(2a)$ in constructing the model predictions. The variation in the experimental data about the model prediction represents systematic variation in these parameters.

Finally, we note that an empirical approach developed by Buscall¹⁸ is often applied to calculate the interaction potential from elastic modulus data.²³ This approach assumes a lattice geometry and, unlike the perturbation theory here, uses a volume fraction dependent nearest-neighbor separation distance.¹⁷ Calculations using this approach and the overlap potential predict similar order of magnitude values for the elastic moduli at effective volume fractions above 0.74 but yield zero for the elastic modulus at lower effective volume fractions as the brushes are not in contact. Consequently, this empirical approach is known to yield anomalous results for the steric layer geometry.^{23,65}

Conclusions

Electrosteric stabilization of polymer dispersions by a grafted layer of poly(methacrylic acid) has been investigated over a wide range of solvent pH and ionic strength at two concentrations of grafted polymer. At low pH, the brush is collapsed and the addition of salt leads to aggregation. The measured stability ratios for both systems can be described quantitatively by a classical DLVO potential with an effective Hamaker constant. The high-frequency viscosity data can be reduced onto a master curve when plotted against the effective volume fraction determined from the zero shear viscosity. However, deviations from the hard-sphere behavior give clear evidence for hydrodynamic permeability of the polyelectrolyte brush.

(61) Potanin, A. A.; Russel, W. B. *Phys. Rev. E* **1995**, 52, 730.

(62) Frankel, N. A.; Acrivos, A. *Chem. Eng. Sci.* **1967**, 22, 847.

(63) No master curve is obtained by applying the well-known hard-sphere scaling (plot of $G' a^3/k_B T$ vs ϕ_{eff}).

(64) Nichol, L. W.; Ogston, A. G.; Preston, B. N. *Biochem. J.* **1967**, 102, 407.

(65) Duits, M. H. G.; Nommensen, P. A.; van den Ende, D.; Mellema, J. *Colloids Surf., A* **2001**, 183–185, 335.

The high-frequency modulus data can be collapsed onto a master curve according to a simple osmotic brush overlap model using the same effective volume fraction. The osmotic overlap potential combined with a rigorous hard-sphere perturbation theory quantitatively *predicts* the measured G_∞ values using only independently measured parameters. In conclusion, we find that despite the complex interplay between electrostatic interactions controlling the solubility and flexibility of the polyelectrolyte brush and steric interactions, the interparticle interaction due to the electrosteric layer can be described simply by the osmotic pressure induced by the overlap of the stabilizing layers.

Acknowledgment. N.J.W. acknowledges partial financial support from the International Fine Particle Research Institute (IFPRI) and useful discussions with S. Elliot and W.B. Russel. Mr. Weissgerber is gratefully acknowledged for help with the synthesis of the model dispersions.

Symbols used

a	Radius of particle core
$a_{\text{DLS}}, a_{\eta 0}$	Particle radii determined by DLS and zero shear viscosity ($a_{\eta 0} = a + L$)
A, A_{eff}	Hamaker constant and effective Hamaker constant
b	Factor to calculate ζ for intermediate κa values
c, d, k	Calibration constants of torsional resonator
$\Delta D, \Delta F$	Change of width of resonance curve of torsional resonator relative to air and shift of resonance frequency relative to air
D_{eff}	Effective hard-sphere diameter (see eq 9)
e	Electron charge
f	Factor to convert mass fraction into effective volume fraction (see eq 13)
$g(r), g_{\text{HS}}(r)$	General radial distribution function and that for effective hard spheres

$G(H)$	Hydrodynamic interactions
G_∞	High-frequency modulus
H	Distance between the solid surfaces of particles ($H = r - 2a$)
k_B	Boltzmann constant
L	Thickness of brush (see Table 1)
M_W	Molecular weight of polymer (7000 g/mol)
r	Distance between particle cores
T	Absolute temperature
$V_t, V_R, V_A, V_{\text{Osm}}, V_{\text{VR}}$	Total, electrostatic, van der Waals, osmotic, and elastic brush deformation interaction potentials ($V_t = V_R + V_A + V_{\text{Osm}} + V_{\text{VR}}$)
w	Weight ratio of particle to particle core (1.05 or 1.08)
W	Stability factor (see eq 14)
z	Valency of counterions
d	Mesh size of hairy layer
ϵ	Relative dielectric constant of solvent
ϵ_0	Dielectric constant of vacuum
ζ	Zeta potential
η'_∞	High-frequency viscosity
κ	Inverse Debye screening length
μ	Viscosity of solvent
μ_e	Electrophoretic mobility
ν_1	Volume of one solvent molecule (0.03 nm ³)
ρ_S, ρ_P, ρ	Density of sample, of polymer hairs, and of particle cores (1.05 g/mL)
ϕ	Volume fraction of particles
$\phi_{\text{core}}, \phi_{\text{eff}}, \phi_{\text{max}}$	Volume fraction of core, effective hard-sphere volume fraction, and maximum volume fraction (=0.58)
ϕ_P	Volume fraction of polymer in outer layer (see Table 1)
χ	Flory–Huggins solvency parameter of polymer (0.485)
ψ_d	Diffuse potential (assumed to be equal to ζ)
LA015734J	